Springer Series in Materials Science 148

Tomoyuki Kakeshita
Takashi Fukuda
Avadh Saxena
Antoni Planes *Editors*

Disorder and Strain-Induced Complexity in Functional Materials

Springer

Springer Series in
MATERIALS SCIENCE 148

Springer Series in

MATERIALS SCIENCE

The Springer Series in Materials Science covers the complete spectrum of materials physics, including fundamental principles, physical properties, materials theory and design. Recognizing the increasing importance of materials science in future device technologies, the book titles in this series reflect the state-of-the-art in understanding and controlling the structure and properties of all important classes of materials.

Please view available titles in *Springer Series in Materials Science*
on series homepage http://www.springer.com/series/856

T. Kakeshita
T. Fukuda
A. Saxena
A. Planes
Editors

Disorder and Strain-Induced Complexity in Functional Materials

With 177 Figures

Springer

Editors

Professor Tomoyuki Kakeshita
Professor Takashi Fukuda
Osaka University, Graduate School of Engineering, Division of Materials and Manufacturing
Yamada-oka, Suita 2-1, 565-0871 Osaka, Japan
E-mail: kakeshita@mat.eng.osaka-u.ac.jp, fukuda@mat.eng.osaka-u.ac.jp

Dr. Avadh Saxena
Los Alamos National Laboratory
Theoretical Division, T-4, MS B262
Los Alamos, NM 87545, USA
E-mail: avadh@lanl.gov

Professor Antoni Planes
Universitat de Barcelona
Departament d'Estructura i Constituents
de la Matèria
Facultat de Física
Diagonal 647, 08028 Barcelona, Spain
E-mail: toni@ecm.ub.es

Series Editors:

Professor Robert Hull
University of Virginia
Dept. of Materials Science and Engineering
Thornton Hall
Charlottesville, VA 22903-2442, USA

Professor Jürgen Parisi
Universität Oldenburg, Fachbereich Physik
Abt. Energie- und Halbleiterforschung
Carl-von-Ossietzky-Straße 9–11
26129 Oldenburg, Germany

Professor Chennupati Jagadish
Australian National University
Research School of Physics and Engineering
J4-22, Carver Building
Canberra ACT 0200, Australia

Dr. Zhiming Wang
University of Arkansas
Department of Physics
835 W. Dicknson St.
Fayetteville, AR 72701, USA

Professor R. M. Osgood, Jr.
Microelectronics Science Laboratory
Department of Electrical Engineering
Columbia University
Seeley W. Mudd Building
New York, NY 10027, USA

Springer Series in Materials Science ISSN 0933-033X
ISBN 978-3-642-20942-0 e-ISBN 978-3-642-20943-7
DOI 10.1007/978-3-642-20943-7
Springer Heidelberg Dordrecht London New York

Library of Congress Control Number: 2011936130

Preface

There is a paradigm shift in our understanding of the properties and behaviour of complex functional materials with multiple ordered phases and competing interactions. One novel aspect is that the underlying lattice provides an elastic template on which charge, spin, dipolar and other degrees of freedom couple to provide a number of emergent functionalities. The role of disorder in the presence of long-range dipolar and elastic forces is to lead to nanoscale inhomogeneity, which is responsible for the observed behaviour as well as frustration in the material – thus a strong sensitivity to external perturbations and possibly glassy response in certain regimes as well as anomalous avalanche phenomena.

This book brings together an emerging consensus on our understanding of the complex functional materials including ferroics, perovskites, multiferroics and magnetoelastics. The common theme is the existence of many competing ground states and frustration as a collusion of spin, charge, orbital and lattice degrees of freedom in the presence of disorder and (both dipolar and elastic) long-range forces. An important consequence of the complex unit cell and the competing interactions is that the emergent materials properties are very sensitive to external fields, thus rendering these materials with highly desirable, technologically important applications enabled by cross-response.

The idea for this book was born at the workshop *Jim Krumhansl Symposium: Complex Materials at the Cross-Roads* held at Osaka, Japan, during November 9–13, 2008. This workshop was a sequel to a previous workshop on *Interplay of Magnetism and Structure in Functional Materials* held at Benasque, Spain, during February 9–13, 2004. The Benasque workshop formed the basis of a book (*Magnetism and Structure in Functional Materials*, Springer, 2005), which was dedicated to Jim Krumhansl, a retired professor from Cornell University who passed away in May 2004. Much of the research reported in this as well as in the previous book was inspired by Prof. Krumhansl's overarching vision identifying common themes between solid-state physics, materials science and biology.

The topics covered in the present book are interdisciplinary in nature written by researchers from physics, materials science and engineering backgrounds.

Therefore, the book is addressed to both the experts and researchers getting into the field of functional materials with disorder and glassy behaviour including graduate students. It contributes to the fields of physics, materials science and nanotechnology. In general, the book represents a developing subject.

The carefully chosen 15 chapters written by internationally recognized experts in their respective fields cover general introduction to ferroics and multiferroics, principles of emergent complexity in materials science with a particular emphasis on magnetic shape memory alloys, glassy phenomena including strain glass and martensites, soft electronic matter, hysteresis and avalanches, high-resolution structural and magnetic visualization techniques, neutron scattering and shuffle-based transitions, defects in ferroelectrics and other ferroic materials, precursor phenomena, magnetostrucutral coupling and magnetocaloric properties, Heusler materials and magnetic martensites as well as first principles and mesoscopic modelling. Beyond illustrating some common threads (such as metastability, nonlinearity and disorder) between biological and materials functionality, the book concludes with a chapter that lays out clearly the future research directions.

Each chapter reviews the current state of the topic and provides sufficient background material for a graduate student or a new researcher to get started in this exciting field. At the same time, each chapter provides open questions for the experts to ponder and advance the field further.

Overall, the book provides an emergent paradigm shaped by the many advances made over the past decade in synthesis, characterization, modelling and fundamental understanding as well as technological applications of a variety of complex functional materials.

We gratefully acknowledge financial support from the Global COE Program "Center of Excellence (COE) for Advanced Structural and Functional Materials Design" at the University of Osaka (Suita campus), Japan. We thank Ms. Yuko Kuroda for her careful assistance in editing the book.

Osaka, Japan — *Tomoyuki Kakeshita*
Osaka, Japan — *Takashi Fukuda*
Los Alamos, USA — *Avadh Saxena*
Barcelona, Spain — *Antoni Planes*

Contents

1 Domain Boundary Engineering in Ferroic and Multiferroic Materials: A Simple Introduction 1
Ekhard K.H. Salje and Jason C. Lashley
1.1 Introduction 1
1.2 Multiferroic Domain Boundaries 2
1.3 Highly Conducting Interfaces 7
1.4 The Dynamics of Domain Movement and Ferroic Switching 9
1.5 Conclusions 15
References 16

2 Phase Diagrams of Conventional and Inverse Functional Magnetic Heusler Alloys: New Theoretical and Experimental Investigations 19
P. Entel, M.E. Gruner, A. Hucht, A. Dannenberg, M. Siewert, H.C. Herper, T. Kakeshita, T. Fukuda, V.V. Sokolovskiy, and V.D. Buchelnikov
2.1 Introduction and Computational 20
2.2 Crystal Structures of Half- and Full-Heusler alloys 21
2.3 Phase Diagrams of $Ni_2Mn_{1+X}Z_{1-X}$ (Z=Ga, In, Sn, Sb) Heusler alloys 25
2.4 Phase Diagrams of $Ni_{2+x}Mn_{1-x}Z$ (Z= Ga, In, Sn, Sb) Heusler alloys 30
2.5 Phase Diagrams of $Co_2Ni_{1-X}Z_{1+X}$ (Z= Ga, Zn) Heusler alloys 33
2.6 Conclusions and Future Aspects of Magnetic Heusler alloys 41
References 43

3 Ni–Mn–X Heusler Materials 49
Ryosuke Kainuma and Rie Y. Umetsu
3.1 Introduction 49
3.2 Atomic Ordering and Magnetic Properties in $Ni_2Mn(Ga_xAl_{1-x})$ Alloys 50
3.2.1 Atomic Ordering 51
3.2.2 Magnetic Properties 52
3.3 Magnetic Properties in Off-Stoichiometric $Ni_2Mn_{1+y}In_{1-y}$ Alloys 55
3.4 Martensitic Transformation and Magnetic Properties in NiMnIn Alloy 58
3.5 Concluding Remarks 62
References 63

4 Magnetic Interactions Governing the Inverse Magnetocaloric Effect in Martensitic Ni–Mn-Based Shape-memory Alloys 67
S. Aksoy, M. Acet, T. Krenke, E.F. Wassermann, M. Gruner, P. Entel, L. Mañosa, A. Planes, and P.P. Deen
4.1 Introduction 68
4.2 The Inverse Magnetocaloric Effect Around a Structural Transitions in a Ferromagnetic System 68
4.2.1 Conventional and Inverse Magnetocaloric Effects in $Ni_{50}Mn_{34}In_{16}$ 70
4.2.2 Magnetic Coupling in Ni–Mn-Based Martensitic Heusler Alloys 71
4.2.3 Magnetic Exchange Constants in Ni–Mn-Based Martensitic Heusler Alloys 74
4.3 Conclusion 75
References 76

5 Magnetic Field-Induced Strain in Ferromagnetic Shape Memory Alloys Fe-31.2Pd, Fe_3Pt, and Ni_2MnGa 79
Takashi Fukuda and Tomoyuki Kakeshita
5.1 Introduction 79
5.2 Martensitic Transformation in Fe-31.2Pd, Fe_3Pt, and Ni_2MnGa 81
5.3 Magnetic Field-Induced Strain in Fe-31.2Pd, Fe_3Pt, and Ni_2MnGa 82
5.4 Condition for Rearrangement of Martensite Variants by Magnetic Field 86
5.5 Origin of Martensitic Transformation in Fe_3Pt 90
5.6 Summary 93
References 93

6 Soft Electronic Matter: Inhomogeneneous Phases in Strongly Correlated Condensed Matter 95
Peter B. Littlewood
6.1 Introduction 95
6.2 A Microscopic View 96
6.3 Example 1: La_2NiO_4 99
6.4 Example 2: Colossal Magnetoresistance in Manganites 100
6.4.1 The Basics: Double Exchange and Jahn–Teller 100
6.4.2 Competing and Cooperating Phases in Manganites 103
6.4.3 Ginzburg–Landau Theory for Manganites 105
6.5 Example 3: Superconductivity and Magnetism in $CeCoIn_5$ 108
6.6 Concluding Remarks 110
References 110

7 Defects in Ferroelectrics 113
Wenwu Cao
7.1 Introduction 113
7.2 Vacancies in Perovskite Ferroelectric Materials 115
7.3 Doping of Aliovalent Defects 117
7.4 Defects and Dielectric Properties 119
7.5 Grain Boundary and Positive Temperature Coefficient Resistor 122
7.6 Domain Walls as a Type of Mobile Defects 125
7.7 Size Effects and Surface in Ferroelectric Materials 129
7.8 Summary 131
References 132

8 High-Resolution Visualization Techniques: Structural Aspects 135
D. Schryvers and S. Van Aert
8.1 Earlier Results on Tweed Patterns in Ni–Al 136
8.2 Matrix Deformation and Depletion from Precipitation in Ni–Ti 137
8.3 Minimal Strain at Austenite – Martensite Interface 140
8.4 Internal Strain Control in Ni–Ti Micro-Wires 142
8.5 Strain Effects in Metallic Nano-beams 142
8.6 Future Prospects 144
References 148

9 High-Resolution Visualizing Techniques: Magnetic Aspects 151
Yasukazu Murakami
9.1 Introduction 151
9.2 Magnetic Imaging by TEM 152
9.2.1 Lorentz Microscopy 153
9.2.2 Electron Holography 154
9.2.3 Instrumentation for Magnetic Domain Observations 156
9.3 Study of Magnetic Microstructure in Colossal Magnetoresistive Manganite 157
9.3.1 Ferromagnetic Domain Nucleation and Growth 158

9.3.2 Determination of Magnetic Parameters of a Nanoscale Region 162
9.4 Magnetic Imaging of Ferromagnetic Shape-Memory Alloys 164
9.4.1 Impact of APBs on the Local Magnetization Distribution 165
9.4.2 Magnetic Pattern Formation Triggered by Premartensitic Lattice Anomaly 169
9.5 Concluding Remarks 172
References 173

10 Understanding Glassy Phenomena in Materials 177
David Sherrington
10.1 Introduction 177
10.2 Spin Glasses: A Brief Review 178
10.3 Martensites 181
10.4 Relaxors 188
10.5 Models, Simulations and Analysis 193
10.6 Conclusion 195
References 197

11 Strain Glass and Strain Glass Transition 201
Xiaobing Ren
11.1 Disorder–Order and Disorder–Glass Transition in Nature: Anticipation of a Strain Glass Transition and Strain Glass 201
11.2 Phase Diagram of Strain Glass: Crossover from LRO to Glass Due to Point Defects 204
11.3 Signatures of Strain Glass and Analogy with Other Glasses 207
11.4 Novel Properties of Strain Glass 211
11.5 Origin of Strain Glass and Theoretical Modeling/Simulations 214
11.6 Strain Glass as a Solution to Several Long-Standing Puzzles About Martensite 219
11.7 Summary 223
References 223

12 Precursor Nanoscale Textures in Ferroelastic Martensites 227
Pol Lloveras, Teresa Castán, Antoni Planes, and Avadh Saxena
12.1 Introduction 227
12.2 Structural Precursor Textures in Cubic Ferroelastics 230
12.2.1 Tweed Textures 230
12.2.2 Effect of Elastic Anisotropy on the Morphology of Structural Precursor Nanostructures 232
12.3 Phenomenological Modeling 235

12.4 Numerical Simulation Results 237
12.4.1 Effect of the Elastic Anisotropy on Structural Precursors: From Cross-Hatched to Mottled Morphology 238
12.4.2 Effect of the Disorder: Frozen Glass State 240
12.4.3 Thermomechanical Behaviour 242
12.5 Conclusions 243
References 244

13 Metastability, Hysteresis, Avalanches, and Acoustic Emission: Martensitic Transitions in Functional Materials 249
Martin-Luc Rosinberg and Eduard Vives
13.1 Introduction 249
13.2 What Can We Learn from Simple Models? 251
13.2.1 Relationship Between Hysteresis and the Distribution of Metastable States 252
13.2.2 Influence of the Driving Mechanism and the Effect of Long-Range Forces 256
13.3 What Can We Learn from Acoustic Emission Detection? 258
13.3.1 Pulse-Counting Technique 259
13.3.1.1 Transition Temperature 260
13.3.1.2 Athermal and Adiabatic Character of the Transition 260
13.3.1.3 Learning 261
13.3.1.4 Dependence on the Driving Mechanism 262
13.3.1.5 Correlation with Calorimetry 263
13.3.2 Statistical Analysis of Single Events 264
13.3.2.1 Exponent Universality Classes 265
13.3.2.2 Learning Process 266
13.3.2.3 Influence of the Driving Mechanism 268
13.3.3 Future Trends for the AE Technique in the Study of Structural Transitions 269
13.4 Concluding Remarks 269
References 270

14 Entropy–Driven Conformations Controlling DNA Functions 273
A.R. Bishop, K.Ø. Rasmussen, A. Usheva, and Boian S. Alexandrov
14.1 Introduction 274
14.2 Transcription Initiation, Transcriptional Start Sites, and DNA Breathing Dynamics 275
14.3 DNA Repair 283
14.4 Bioinformatics and DNA Breathing Dynamics 286
14.5 Conclusions 288
References 289

15 Conclusion and Outlook 293
Per-Anker Lindgård
15.1 Outlook 299
References 300

Index 303

Contributors

Mehmet Acet Physics Department, University of Duisburg-Essen, 47048 Duisburg, Germany, mehmet.acet@uni-due.de

S. Aksoy Faculty of Engineering & Natural Sciences, Sabanci University, 34956 Istanbul, Turkey, saksoy@sabanciuniv.edu

Boian S. Alexandrov Theoretical Division, Los Alamos National Laboratory, Los Alamos, New Mexico, USA, boian@lanl.gov

A. R. Bishop Theoretical Division, Los Alamos National Laboratory, Los Alamos, NM, USA, arb@lanl.gov

V.D. Buchelnikov Condensed Matter Physics Department, Chelyabinsk State University, 454021 Chelyabinsk, Russia, buche@csu.ru

Wenwu Cao Department of Mathematics, The Pennsylvania State University, University Park, PA 16802, USA, cao@math.psu.edu

Teresa Castán Facultat de Física, Departament d'Estructura i Constituents de la Matèria, Universitat de Barcelona, Diagonal 647, 08028 Barcelona, Catalonia, Spain

Institut de Nanociència i Nanotecnologia, Universitat de Barcelona, Catalonia, Spain, teresa@ecm.ub.es

A. Dannenberg Faculty of Physics & CeNIDE, University Duisburg-Essen, 47048 Duisburg, Germany, antje@thp.uni-duisburg.de

P.P. Deen European Spallation Source ESS AB P.O Box 176, SE-221 00 Lund, Sweden, pascale.deen@esss.se

Peter Entel Faculty of Physics & CeNIDE, University Duisburg-Essen, 47048 Duisburg, Germany, entel@thp.uni-duisburg.de

Takashi Fukuda Graduate School of Engineering, Osaka University, Suita, Osaka 565-0871, Japan, fukuda@mat.eng.osaka-u.ac.jp

M.E. Gruner Faculty of Physics & CeNIDE, University Duisburg-Essen, 47048 Duisburg, Germany, Markus.Gruner@uni-due.de

H.C. Herper Faculty of Physics & CeNIDE, University Duisburg-Essen, 47048 Duisburg, Germany, heike.herper@uni-due.de

A. Hucht Faculty of Physics & CeNIDE, University Duisburg-Essen, 47048 Duisburg, Germany, fred@thp.uni-duisburg.de

Ryosuke Kainuma Department of Materials Science, Tohoku University, Sendai, Japan, kainuma@material.tohoku.ac.jp

Tomoyuki Kakeshita Graduate School of Engineering, Osaka University, Suita, Osaka 565-0871, Japan, kakesita@mat.eng.osaka-u.ac.jp

T. Krenke Thyssen Krupp Electrical Steel GmbH, D-45881 Gelsenkirchen, Germany, thorsten.krenke@thyssenkrupp.com

Jason C. Lashley Los Alamos National Laboratories, Los Alamos, NM USA, j.lash@lanl.gov

Per-Anker Lindgård Materials Research Division, Risó, DTU, National Laboratory for Sustainable Energy, 4000-Roskilde, Denmark, hanne.frederiksen@mail.tele.dk

Peter B. Littlewood Cavendish Laboratory, Cambridge University, JJ Thomson Avenue, Cambridge CB3 0HE, UK, pbl21@cam.ac.uk

Pol Lloveras Facultat de Física, Departament d'Estructura i Constituents de la Matèria, Universitat de Barcelona, Diagonal 647, 08028 Barcelona Catalonia, Spain

Institut de Nanociència i Nanotecnologia, Universitat de Barcelona, Catalonia, Spain, pol@ecm.ub.es

L. Mañosa Departament d'Estructura i Constituents de la Matèria, Facultat de Física, Universitat de Barcelona Diagonal 647, 08028 Barcelona, Catalonia (Spain), lluis@ecm.ub.es

Yasukazu Murakami Institute of Multidisciplinary Research for Advanced Materials, Tohoku University, Sendai, Japan, murakami@tagen.tohoku.ac.jp

Antoni Planes Facultat de Física, Departament d'Estructura i Constituents de la Matèria, Universitat de Barcelona, Diagonal 647, 08028 Barcelona Catalonia, Spain

Institut de Nanociència i Nanotecnologia, Universitat de Barcelona, Catalonia, Spain, toni@ecm.ub.es,antoniplanes@ub.edu

Kim Ø. Rasmussen Theoretical Division, Los Alamos National Laboratory, Los Alamos, NM, USA, kor@lanl.gov

Xiaobing Ren Ferroic Physics Group, National Institute for Materials Science, Tsukuba, Japan, REN.Xiaobing@nims.go.jp

Martin-Luc Rosinberg Laboratoire de Physique Théorique de la Matière Condensée, Université Pierre et Marie Curie, 4 Place Jussieu, 75252 Paris, France, mlr@lptmc.jussieu.fr

Ekhard K.H. Salje University of Cambridge, Downing Street, Cambridge CB 2 3EQ, Cambridge UK, es10002@esc.cam.ac.uk

Avadh Saxena Theoretical Division, Los Alamos National Laboratory, Los Alamos, NM 87545, USA

Institut de Nanociència i Nanotecnologia, Universitat de Barcelona, Barcelona Spain, avadh@lanl.gov

Dominique Schryvers EMAT, University of Antwerp, Groenenborgerlaan 171, 2020 Antwerp, Belgium, nick.schryvers@ua.ac.be

David Sherrington Santa Fe Institute, 1399 Hyde Park Road, Santa Fe, NM 87501, USA

Rudolf Peierls Centre for Theoretical Physics, University of Oxford, 1 Keble Rd., Oxford OX1 3NP, UK, d.sherrington1@physics.ox.ac.uk

M. Siewert Faculty of Physics & CeNIDE, University Duisburg-Essen, 47048 Duisburg, Germany, mario@thp.uni-due.de

V.V. Sokolovskiy Condensed Matter Physics Department, Chelyabinsk State University, 454021 Chelyabinsk, Russia, vsokolovsky84@mail.ru

Rie Y. Umetsu Institute for Materials Research, Tohoku University, Sendai, Japan, rieume@imr.tohoku.ac.jp

Anny Usheva Beth Israel Deaconess Medical Center, Harvard Medical School, Boston, MA, USA, ausheva@bidmc.harvard.edu

Sandra Van Aert EMAT, University of Antwerp, Groenenborgerlaan 171, 2020 Antwerp, Belgium, sandra.vanaert@ua.ac.be

Eduard Vives Facultat de Física, Departament d'Estructura i Constituents de la Materia, Universitat de Barcelona, Martí i Franquès 1, 08028 Barcelona, Catalonia, Spain

Institut de Nanociència i Nanotecnologia (IN2UB), Universitat de Barcelona, Barcelona, Catalonia, Spain

Department of Physics, University of Warwick, Coventry CV4 7AL, UK, eduard@ecm.ub.es

E.F. Wassermann Physics Department, University of Duisburg-Essen, D-47048 Duisburg, Germany, eberhard.wassermann@uni-due.de

Chapter 1
Domain Boundary Engineering in Ferroic and Multiferroic Materials: A Simple Introduction

Ekhard K.H. Salje and Jason C. Lashley

Abstract Multiferroic behavior is commonly described as a bulk phenomenon where, at least, two of the three ferroic properties, ferromagnetism, ferroelectricity, and ferroelasticity, coincide. This notion is enlarged to contain as another "useful" property electrical conductivity. While bulk applications are potentially useful, we describe the recent development where the same properties are restricted to domain boundaries or interfaces, while the adjacent domains are not active elements themselves. This means that the information is restricted to thin, nearly two-dimensional slabs of some 2 nm thickness. The information density is, thus, extremely high, while conducting interfaces can serve as wires to connect the active elements. In this chapter, we discuss the underlying physical principles for the "engineering" of interfacial multiferroics.

1.1 Introduction

Multiferroicity combines at least two of the three ferroic properties of a material: ferroelasticity, ferroelectricity, or ferromagnetism. Its investigation has a long tradition with significant work on boracites in the 1960s [1] and a continuous stream of activities on ceramics with perovskite-like structures [2–8]. In addition, it was realized that "ferroelastics" and "martensites" describe the same materials properties that have simply different historic traditions for their naming (so that "ferroelastic" alloys are usually called "martensites" and have often, but not

E.K.H. Salje (✉)
University of Cambridge, Downing Street, Cambridge CB 2 3EQ, Cambridge, UK
e-mail: es10002@esc.cam.ac.uk

J.C. Lashley
Los Alamos National Laboratory, Los Alamos, NM, USA
e-mail: j.lash@lanl.gov

T. Kakeshita et al. (eds.), *Disorder and Strain-Induced Complexity in Functional Materials*, Springer Series in Materials Science 148,
DOI 10.1007/978-3-642-20943-7_1, © Springer-Verlag Berlin Heidelberg 2012

always, step-wise phase transitions [9], while ceramics and minerals, which have "martensitic" properties, are usually called "ferroelastics"). Magnetic martensites, for example, are multiferroics and follow the same physical mechanism as the very large number of ferromagnetic *cum* ferroelastic ceramics.

The motivation for the investigation of multiferroic materials is that better memory devices can be made from such compounds [10, 11]. For this purpose, ferroelasticity is of minor importance because reading/writing mechanisms will rely on magnetic or electric fields so that the key for the development of multiferroics is the combination of ferroelectric and ferromagnetic properties. The role of ferroelasticity is nevertheless often a key for the performance of such devices: coupling between different ferroic properties can be "strain-induced" where both properties couple strongly with some lattice distortion (via magnetostriction and electrostriction or piezoelectricity, etc.) and, thus, couple with each other. Strain-induced coupling occurs on an atomic scale [12, 13] or on a mesoscopic scale [14–16], whereby the latter allows further development of enhanced strains via microengineering resolution patterning and processes.

Current work on structural multiferroics was revived with work focussing mainly on $BiFeO_3$ [17–20]. Two further developments have occurred after 2000, which may lead to even more effective multiferroic device materials. Firstly, coupling with charge carriers is now subject to much research. Here, the combination between a magnetically or electrically written signal and its reading via high conductivity regions in a material has become an attractive proposition [21–25]. Such regions can be grain boundaries, interfaces, or twin boundaries or be part of exsolution patterns or amorphized/glassy clusters [26–28]. The second development leads this idea even further: why not to take such interfacial regions as active elements of the multiferroic properties themselves. This restricts the size of the active element to a few nm in thickness, while the crystal simply serves as matrix in which such heterostructures are located. It is the purpose of this introduction to highlight some of the developments that lead to the emerging field of "domain boundary engineering" which, potentially, brings the size of active elements, say in memory devices, from currently 0.1 μm to well below 50 nm and also allows a truly 3D arrangement of multiferroic elements.

1.2 Multiferroic Domain Boundaries

Domain boundaries, in particular twin boundaries, which are discussed now, show reduced chemical bonding with many of the structural constituents. With respect to elastic, magnetic, or electric susceptibilities, one expects domain boundaries to be "softer" than the bulk, although such softening can hardly be measured macroscopically because the volume proportion of interfaces is relatively small compared with the bulk. An exception is – in some measure – relaxor materials where the relaxor regions themselves have wall properties (for order–disorder systems) and show indeed strong finite size effects and soft susceptibilities [29–31].

Nevertheless, twin boundaries can reach several parts-per-million of the sample volume so that large signals from internal ferroic properties of the boundaries may even compete with the macroscopic properties of the bulk. The advantage of the localized wall properties is their high information density: they are contained within very thin sheets of twin walls and can be addressed spatially with very high resolution. This means that the storage density of information encrypted in twin walls is extremely high so that wall-related devices could theoretically outperform bulk devices by several orders of magnitude.

The second ingredient is the condition that structural gradients of twin walls extend over several interatomic distances. In Fig. 1.1, a high resolution electron microscopy image of a twin wall in $NdGaO_3$ is shown where the imaging condition was optimized for atoms inside the twin wall, while atoms outside the wall are slightly out of imaging condition by inclination of their lattice plane from the plane of diffraction. The "thickness" of the twin wall can now be estimated by simply counting the number of unit cells in the wall. The resulting wall thickness of ca. 2 nm compares well with results from diffraction experiments at low temperatures in interfaces and surfaces [32–34]. The wall thickness increases when the transition point is approached. Careful analysis of the diffuse diffraction of wall-related signals in $LaAlO_3$ showed that the wall thickness increases according to the predictions of Landau–Ginzburg theory for a second-order phase transition [8, 33]. In first-order martensitic transitions, the effect is smaller although the increase follows still the scaling of the correlation length of the phase transition, which leads to significant increases near the transformation point in compounds such as NiTi and NiTiFe [35, 36].

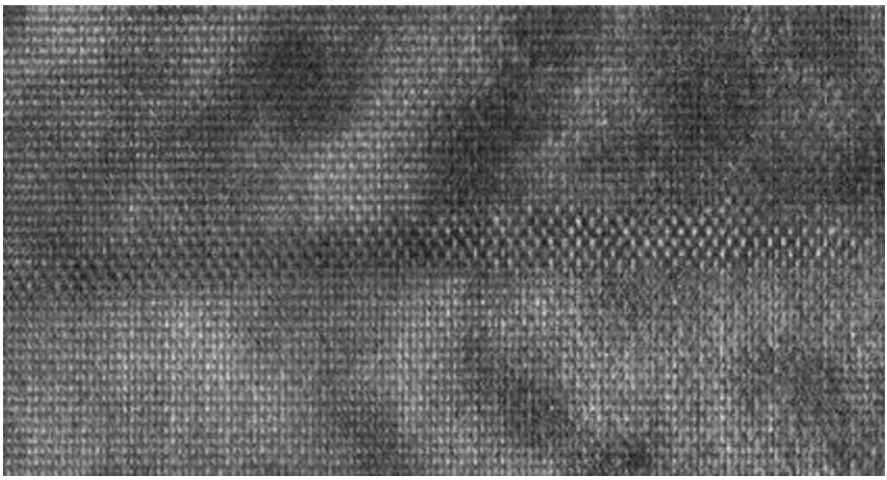

Fig. 1.1 Transmission electron microscopy image of NdGaO3 (Pbnm) near a {101} twin boundary in the middle of the figure. The unit cell is $a = 0.5426$ nm, $b = 0.5502$ nm, and $c = 0.7706$ nm for the orthorhombic cell and $a = b = 0.3864$ nm and $c = 0.3853$ nm for a perovskite-related cell. The thickness of the interface is 2w $\sim$ 6 unit layers or $\sim$2.3 nm (photograph courtesy G. Van Tendeloo, Antwerp)

The discovery of ferroic properties of interfaces is often related to computer simulations for materials design and the theoretical exploration of extreme physical properties in solids. Such research expands from inorganic materials to biological samples in life sciences. We first discuss an example in solid state physics where sizeable spontaneous polarization was predicted in {100} twin walls of $CaTiO_3$, a definitely nonpolar material [37, 38]. Theoretical simulations [39–41] of these walls show an extremely rich texture of the local polarization at and close to the walls. Local distortions include a strong antiferroelectric component, and local nonzero contributions perpendicular to the wall plane, which do not contribute to the macroscopic net dipole moment. Individual Ti displacements of 2 pm off the octahedron center give rise to a net polarization corresponding to a displacement of 0.6 pm in the direction of the bisector of the twin angle. The effect is intrinsically coupled with the appearance of twin boundaries in the matrix, which was already previously identified as locality of oxygen vacancies in $CaTiO_3$ [37, 41].

While indirect evidence for the polar behavior of twin walls has been reported before [42], as well as in antiphase boundaries, APBs [43], and grain boundaries [44], the results in $CaTiO_3$ are very instructive as it was the first clear indication of twin wall polarity and the underlying structural mechanism for the coupling between strain and dipole moments. $CaTiO_3$ is orthorhombic in its low-temperature form (space group Pnma) and is purely ferroelastic. No ferroelectric features have ever been recorded. The TiO_6 octahedron, on the other hand, is well known for its tendency to form polar groups where the Ti position is offcentered with respect to the geometrical center of the surrounding oxygen atoms. Such polar structures exist in compounds such as $BaTiO_3$, $PbTiO_3$, and others. The known competition with octahedral rotation [45] in the tetragonal and orthorhombic phases of $CaTiO_3$ suppresses the off-centering. It is, however, restored when the rotation angle vanishes or when the density of the material decreases. Both conditions are met inside the twin wall and it is thus not entirely unexpected that twin walls should show dipolar moments. What was unknown is the actual size of the polarization and the texture of the polarization field.

To investigate polar ordering in the ferroelastic walls of $CaTiO_3$, numerical simulations were performed based on an atomic-scale description of the walls in which atoms interact via empirically defined forces [37–42]. Periodic boundary conditions were used in three dimensions. Open boundary conditions in the direction perpendicular to the walls would imply surfaces, which would add unwanted complexity to the problem. Two twin walls are needed to conform to periodic boundary conditions. A supercell was built of 26 unit cells in the direction x perpendicular to the walls, six unit cells in the direction perpendicular to the plane of the twin angle (z), and ten unit cells in the bisector of the twin angle y (using the unit cell of the prototypic cubic structure). This gives a total of 7,800 atoms. Figure 1.2 shows the primary order parameter Q as a function of x, in the direction perpendicular to the wall. Q is a measure of the rotation around the y axis of the oxygen octahedra around each titanium atom, appropriately sign corrected. The dashed line indicates the fitted $Q \sim \tan h(x/w)$ functional form which is expected from Landau theory [8]. The wall width lies well within the experimental values

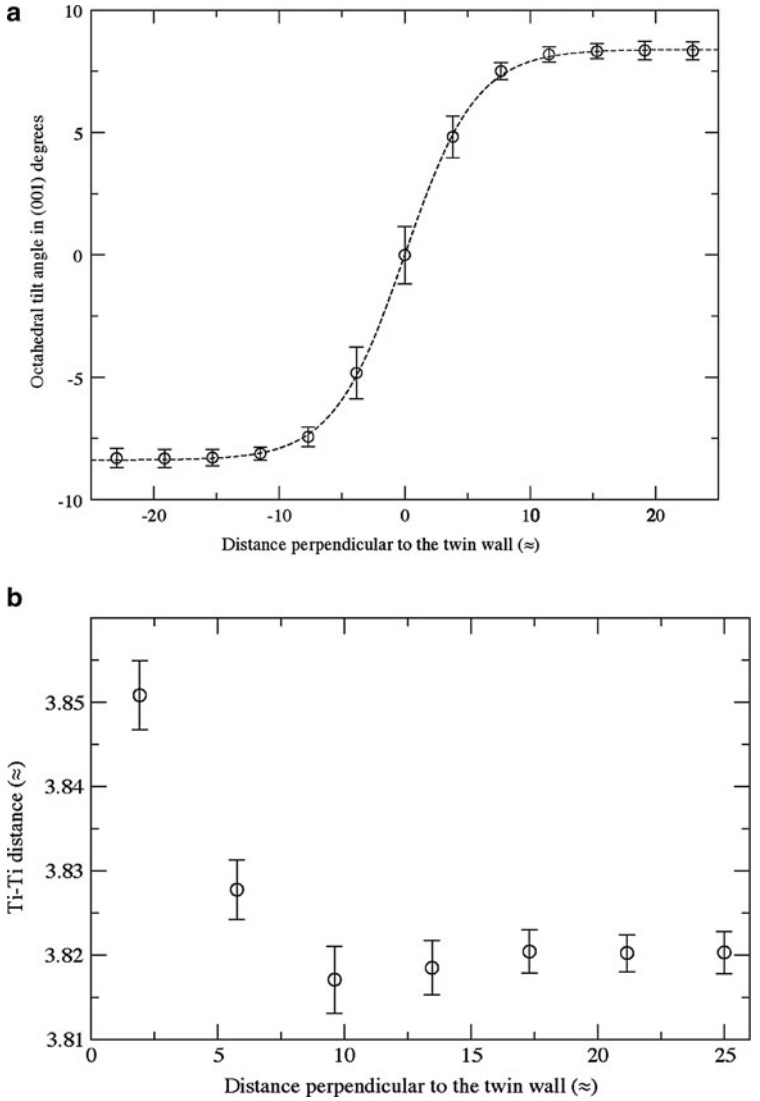

Fig. 1.2 (**a**), (**b**) Profile of the twin wall in $CaTiO_3$. The primary order parameter is the rotation of the TiO_6 octahedra. The twin boundary shows an inversion of the rotation angle (Fig. 1.1a) where the *dotted line* indicates the predictions from Landau–Ginzburg theory. The secondary order parameter is the widening of the unit cell, which is measured by the distance between two adjacent Ti positions. Figure 1.1b shows the increase of the Ti–Ti distance in the wall by ca. 1%, which is sufficient to induce off-centering of the Ti atom from the middle of the octahedra and also an increase of the mobility of defects

as determined previously [33]. The secondary order parameter of interest here is the off-centering of Ti from the center of charge of the corresponding oxygen octahedron. The largest displacements are of 2.0 pm, mostly along the z direction.

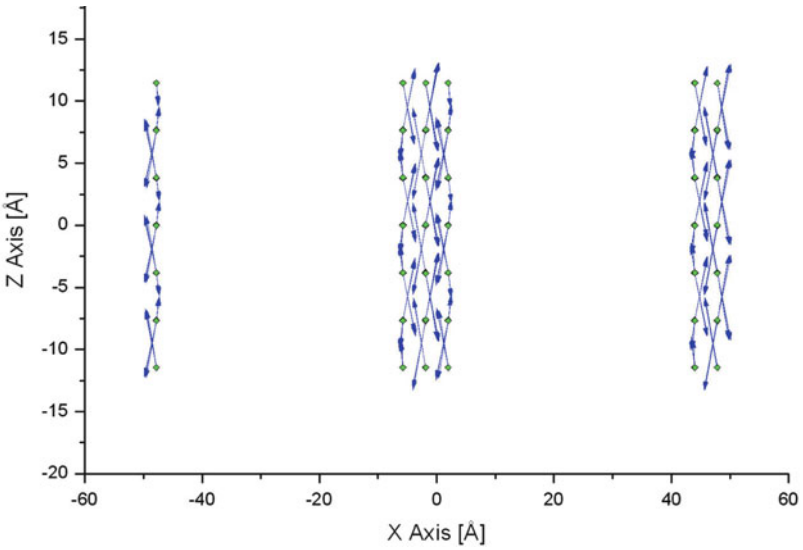

Fig. 1.3 Patterns of the off-centering of Ti from the midpoint of the oxygen octahedra in $CaTiO_3$. The graph shows the displacement patterns in the direction to the twin walls

Two types of off-centering are seen (Fig. 1.3) within the domain wall. The largest component is the one along the z direction antiferroelectric with alternating Ti positions shifted in opposite directions. In contrast, the off-centering along the y direction is ferroelectric and produces a net dipole moment for each domain wall equivalent to a net displacement of 0.6 pm per Ti atom (0.9 pm for the second force field). There is also a smaller antiferroelectric component along the direction perpendicular to the wall, x.

In addition to the appearance of polar properties of the walls, an increase of oxygen vacancies was also predicted. An oxygen vacancy gains ca. 1.1 eV when shifted from the bulk of the material into the twin wall [41]. While this effect is expected from the fact that twin walls in the geological context are known to be decorated by defects, we understand from these calculations that the geometrical requirement for the accommodation of defects may appear negligible, namely, ca.1% increase of a lattice spacing in $CaTiO_3$. Such small changes are typical for twin boundaries and other interfaces so that the observation that dopants are concentrated in interfaces is not unexpected. These localized dopants, on the other hand, can then be used systematically to modify the properties of the walls, e.g., their conductivity or polarity. Doping with magnetic ions may then lead to magnetic properties of the walls, while the same dopants would not necessarily enter the bulk.

The widening of the unit cell at the interface could also lead to a reduction of the local elastic response. This does not mean that the position of a twin wall can be shifted by external forces (which it can), but the compressibility of the wall itself is larger than the equivalent compressibility of the bulk. While such an effect has been seen [40], it appears that the effect is much smaller than could be expected

by the simple reduction of the density in the wall. In fact, the reduction of the relevant elastic modulus as expected by the increase of the distance between nearest neighbous is partly compensated by the decrease of the distance of the next nearest neighbous [46] so that the relaxation of the structure compensates to a large extent the elastic softening due to the swelling of the interface.

1.3 Highly Conducting Interfaces

We have argued that twin walls can attract defects, which leads to the possibility to dope twin boundaries selectively, i.e. to introduce defects into the boundaries but not in the bulk. This possibility was first used to change the conductivity in WO_3 in 1998 [21] with the introduction of Na and oxygen vacancies in twin walls [47–49]. The chemical composition of the walls was very slightly modified (e.g. from WO_3 to $WO_{2.95}$), which induced a metal–insulator transition and, at low temperature, led to the appearance of superconductivity in twin walls. The fact that the dopants follow the trajectories of the twin walls means that nanopatterning of the superconducting structure is possible via the patterning of the twin boundaries and subsequent doping (Figs. 1.4 and 1.5).

Tungsten oxide, WO_3, and its substoichiometric derivatives, WO_{3-x}, are particularly well suited for this research because they display metal–insulator transitions, while they remain thermodynamically stable compounds. They display a multitude of structural phase transitions [50] mainly related to shape changes of the WO_6 octahedra and their rotations within an octahedral network. WO_3 easily releases oxygen and incorporates alkali ions and hydrogen. The facility with which oxygen is released under reducing conditions is less related to the chemical bonding of

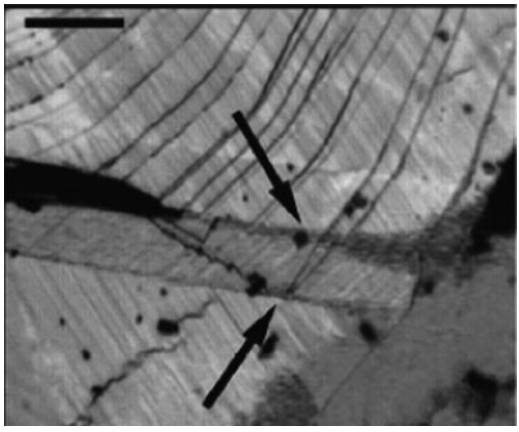

Fig. 1.4 superconducting twin walls (*arrows*) in WO_3 close to the crystal surface. The scale bar in the *top left corner* is 50 μm

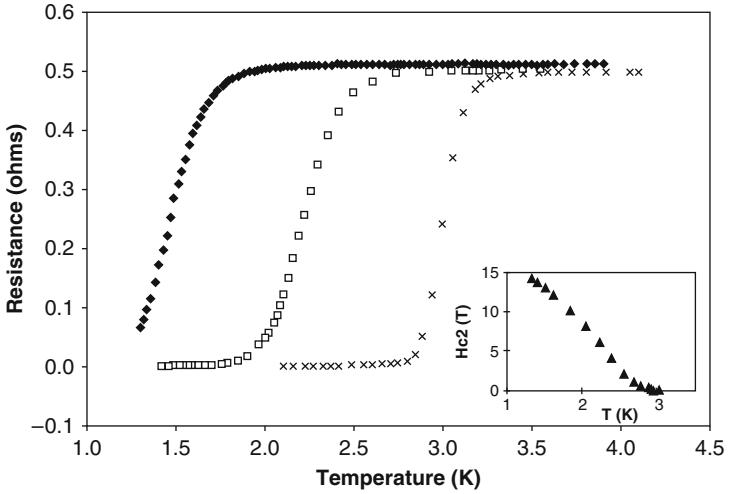

Fig. 1.5 Resistance of the superconducting twin wall in WO_3. The onset of superconductivity is 3 K; the critical field H_{c2} increases to 15 T at low temperatures

oxygen but rather to the low energy required to transfer the valence state of localized surplus electrons on the W^{6+} sites to W^{5+}. This tendency to form W^{5+} states near surfaces was directly confirmed by XPS/UPS experiments [51] and indirectly by STM imaging [52]. These W^{5+} states are not localized, however, and form bi-polarons in the low-temperature phase [53, 54]. WO_3 is a well-known electrochromic, solar cell, and catalytic material; it also displays the remarkable superconducting properties discussed before. Superconducting twin walls in WO_3 are chemically slightly reduced by inserting Na or removing O from the walls. The chemically modified walls (the changes are minor and analytically hard to detect) are then superconducting with a critical field H_{c2} above 15 T and a superconducting transition temperature T_C near 3 K. The surrounding matrix remains insulating so that this arrangement of superconducting twin boundaries with the formation of needle domains and domain junctions is potentially the key for engineering arrays of Josephson junctions and high sensitivity magnetic scanners. In addition, it has been suggested that surface layers, presumably similar to the interfacial structures in WO_3, may display superconductivity at temperatures up to $T_c = 91$ K (Na doping) and 120 K (H doping) [55]. These would constitute extreme values of T_c, which have not been reproduced independently, while the lower value in domain boundaries (3 K in [21]) has been directly observed by transport measurement and subsequently reproduced. In Fig. 1.6, we show the room temperature contrast as measured in AFM and PFM of a WO_3 surface. The highly conducting interfaces are clearly visible. The underlying bulk is piezoelectric, which ensures coupling with electric fields. In addition, it was reported that the ϵ-phase in WO_3 is ferroelectric [50] so that piezoelectric – ferroelectric – superconducting coupling becomes possible.

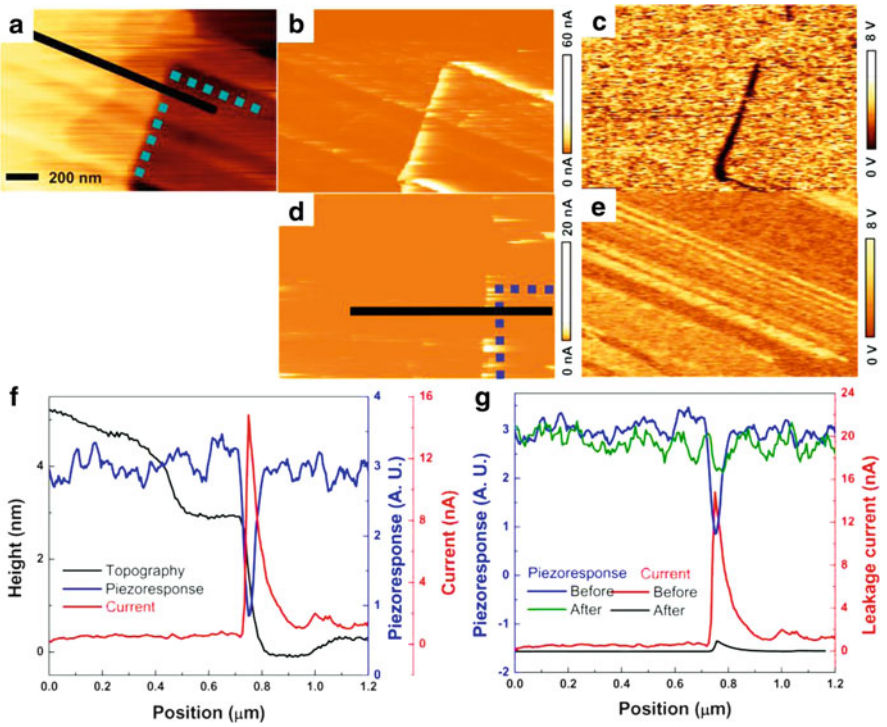

Fig. 1.6 (**a**) Topography, (**b**) current, and (**c**) PFM amplitude images of a freshly reduced WO_{3-x} single crystal. (**d**) Current and (**e**) PFM amplitude images of the same area of the WO_{3-x} single crystal as in (**a**) measured after several weeks. (**f**) Topography, current, and amplitude (piezoresponse) profiles acquired along the *black line* in (**a**), (**b**), and (**c**), respectively. (**g**) Current and amplitude (piezoresponse) profiles before and after an elapsed time of several weeks. The *dotted box* of (**a**) and (**d**) presents the steps to identify the location [56]

1.4 The Dynamics of Domain Movement and Ferroic Switching

If interfaces are taken to be the active elements of a material, the question arises whether such interfaces are stable under external forces or whether their location changes. This will decide their applicability: pinned interfaces will be used according to their internal dynamics, while mobile interfaces will change the size of the adjacent domains and, thus, operate similar classic ferroics where the size of the domains in the various orientations determines the response of a material with respect to external fields.

In multiferroics, the common view is that interfaces can move with external fields in a momentum-driven dynamics. The domains then propagate as classic front propagation [8] for large enough fields. For small field strength, this picture was shown to be wrong, however. Careful measurements under small thermal and elastic driving forces have revealed jerky front propagation and avalanche formation.

This phenomenon is well known in shape-memory alloys where the movement of interfaces between austenite and martensites leads to acoustic emission (AE) similar to Barkhausen-type avalanche behavior where – in the conventional picture – jerky propagation of one interface releases a multitude of other interfaces so that ultimately an avalanche of propagating phase fronts is observed [57]. Theoretically, such avalanches are expected to obey power law distributions [58] and can be considered to be at or near a point of selforganized criticality [59]. While this idea is appealing for its simplicity, it is hard to imagine that the randomness of the various pinning centers in martensites will not extend to extremely low values where pinning can occur only at very low temperatures. In fact, most experiments seem to indicate that pinning, depinning, and acoustic emission (AE) dynamics is a-thermal, which means that it is not thermally activated. A key experiment was recently performed [60] where the transition in a $Cu_{67.64}Zn_{16.71}Al_{15.65}$ shape-memory alloy was investigated calorimetrically, whereby the thermal driving force was minimized. The transition was scanned at rates of some mK/h so that each avalanche could be observed as an individual peak in the latent heat. The resulting DTA curve is shown in Fig. 1.7. It consists of two components: the jerks (Fig. 1.8) and a continuous background.

The entropy of the transition is not affected by the jerks and is the same on heating and cooling. Besides for the strongest avalanches, no memory effect was observed for the individual jerks. The statistical analysis of the jerks is the same as of AE spectra (Fig. 1.8) and follows a power law of the energy of the jerks: $P(E) \sim E^{-\varepsilon}$ with an exponent close to $-\varepsilon \sim -2$. This observation shows that the AE exponents are identical with or close to the energy exponents and not the size exponents (Fig. 1.9).

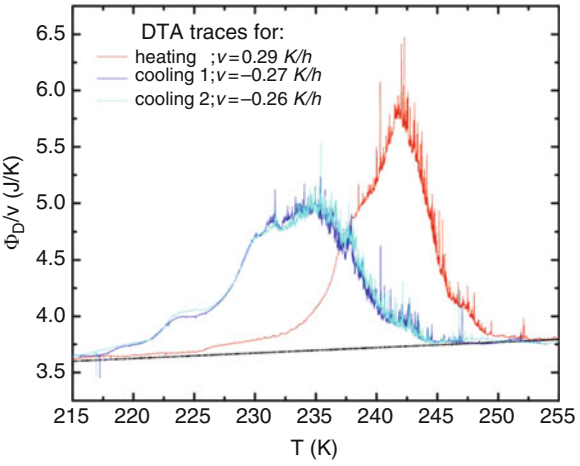

Fig. 1.7 DTA traces for cooling and heating experiments. The heating rate was 0.29 K/h, the cooling rates were 0.27 and 0.26 K/h. Note the coexistence of smooth front propagation and thermal spikes (jerks) even at very low thermal driving forces

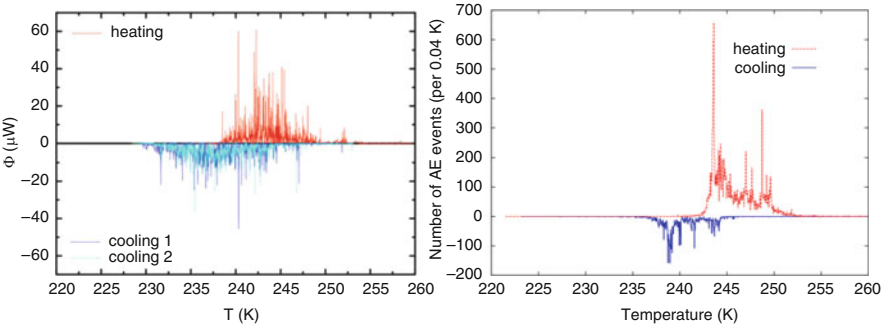

Fig. 1.8 Spikes in the calorimetric measurement after removing the smooth baseline (*left*) and acoustic emission (AE) signals (*right*) of the same sample. The sign of the peaks has been inverted for clarity between heating and cooling experiments [60]

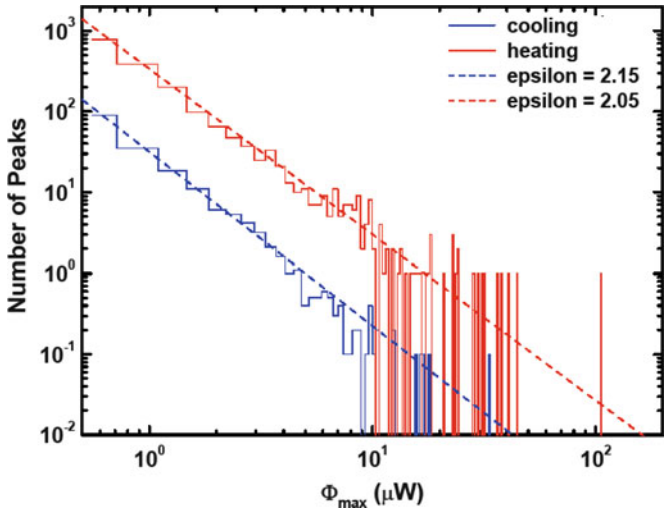

Fig. 1.9 Statistical analysis of the heating and cooling curves of the DTA traces in Fig. 1.3. Data corresponding to cooling experiments have been shifted one decade downward in order to clarify the picture [60]

A direct observation of the jerks in elastic measurements depends on the smallness of the applied forces. The transition in $Cu_{74.08}Al_{23.13}Be_{2.79}$ was investigated in a very careful dynamical mechanical analyzer (DMA) experiment. The frequency of the three-point-bending excitation was chosen as 0.1 Hz, the applied forces were extremely small (<50 mN max. amplitude), and the heating/cooling rate was <0.14 K/h. The mechanical loss is $\sim \tan(\delta)$ and shows spiky avalanche behavior (Fig. 1.10) similar to those in Fig. 1.8. Statistical analysis of the jerks leads again to a power law. The exponent (−1.3) is significantly smaller than the energy exponent of the calorimetric measurement, even though the uncertainty of the fitted exponent

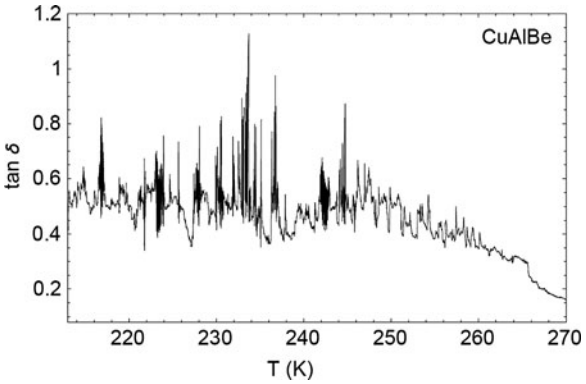

Fig. 1.10 Phase lag tan(δ) of a $Cu_{74.08}$ $Al_{23.13}$ $Be_{2.79}$ single crystal recorded in three-point-bending mode at 0.1 Hz and a heating rate of 0.15 K/h [61]

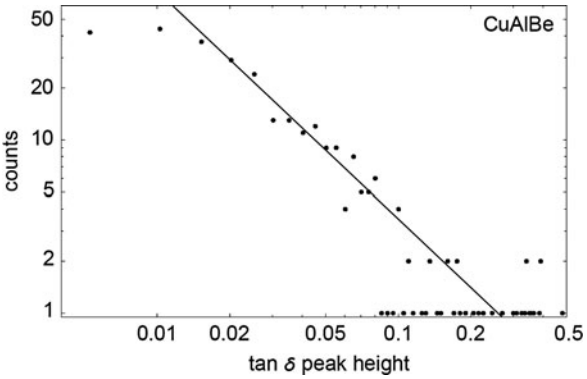

Fig. 1.11 Log–log plot of the peak statistics in Fig. 1.5. The *line* represents the best fit to a power law $P(E) \sim E^{-\varepsilon}$ with $\varepsilon = 1.3$ and an upper bound of 1.6 [61]

is very large. As an upper bound the exponent of -1.6 was estimated in [61]. As the elastic response is measured under oscillatory stress, one may expect that the exponent is related to field binning and related to the amplitude exponent $-\tau$, which was calculated to be in the order of -1.5 in MFT and near -1.3 in simulations [62] (Fig. 1.11).

The movement of interfaces between martensitic variants and ferroelastic twin walls depends theoretically on the dimension of the interface. Planar interfaces have the dimension 2 ($D = 2$), while the tip of a moving needle domain is a line in three dimensions and represents the case $D = 1$. Boundaries well beyond the depinning threshold move freely as solitary waves; their behavior has been well described in the literature [63].

In Fig. 1.12, the trajectory of a needle domain in $LaAlO_3$ is shown. The advancing or retracting needle domain is pinned by defects that are mostly located

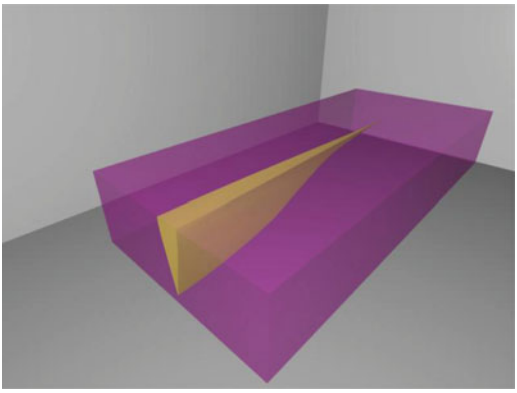

Fig. 1.12 Shape of a needle domain inside the ferroelastic matrix. The advancing front ($D = 1$) is pinned by a small number of defects

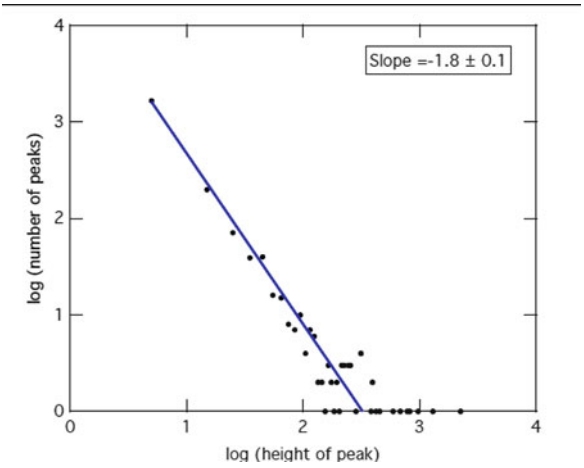

Fig. 1.13 Power law dependence of the energy emission of a single advancing needle domain ($D = 1$). The exponent is estimated to be ~ -1.8

at the advancing edge of the hull-shaped domain. Pinning is then described as the local fixation of a line in three-dimensional space, $D = 1, d = 3$. It is not trivial that pinning should occur at all in this scenario: the Larkin length of the edge in elastic systems is assumed to be large and very strong pinning centers are required in order to obtain the pinning of the advancing needle (Fig. 1.13).

In this context, the recent contribution of Proville [64] is relevant. He showed that in cases where the Larkin length is larger than the system size one can still expect avalanches with a finite depinning force. This observation calls into question the traditional way how the Larkin length is simulated in computer experiments: the elasticity of the interface is simply represented by interatomic springs between

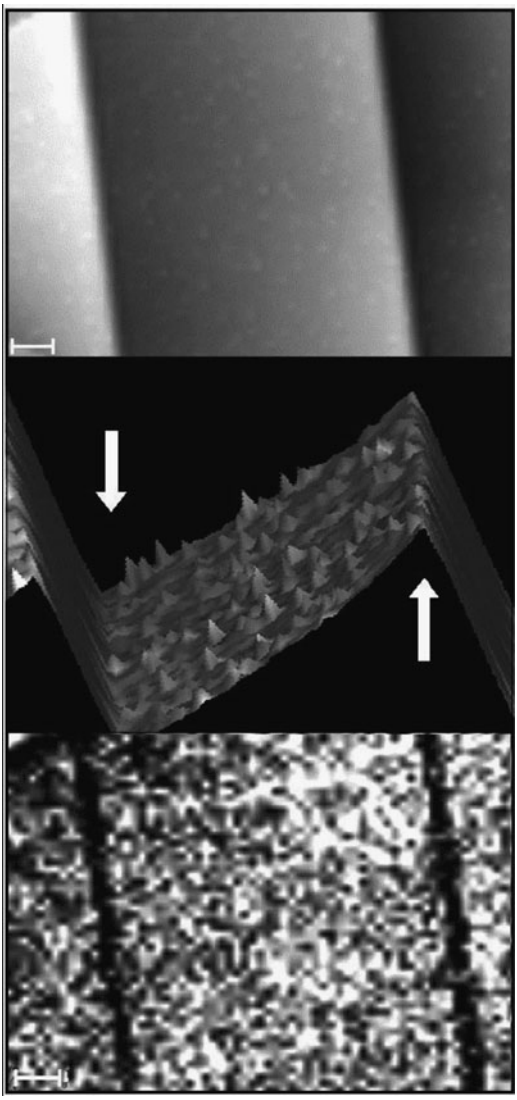

Fig. 1.14 Optical (*top*) and AFM images of twin boundaries in $Pb_3(PO_4)_2$ with high number of Ba defects (courtesy U. Bismayer, University of Hamburg) [33,34]. Scale bar is 6 μm. The pinning by Ba is very weak indicating that the Larkin length is very long

atoms in the wall. This is not the sole obvious mechanism in ferroelastic systems, however. It was shown [65] that the two major forces acting on the interface – in addition to the wall energy itself – are the "anisotropy energy" (which is minimal for walls with an orientation where the compatibility relation is satisfied). Any rotation of a wall segment requires significant energy $\sim \cos\varphi$ (in a local approximation), where φ is the angle between the stress-free equilibrium direction and the actual

direction of the wall segment. The second important energy is the wall "bending energy," which resists any curvature of the wall and is particularly large in case of thick walls [65]. These energies will act against the roughening of walls and ensures that twin walls remain globally planar even under doping conditions, which would normally lead to rough walls in magnetic systems. Such walls would meander in order to take advantage of as many defects as feasible to obtain a maximum pinning force. The AFM image in Fig. 1.9 shows the case of Ba-doped $Pb_3(PO_4)_2$ where no significant pinning is achieved by the addition of the Ba atoms. The moving wall does not meander and remains smooth. It can wrap around defects whenever they encounter such defects or defect clusters. The characteristic length is then given by the geometry of the defect and the details of the elastic interactions and is much longer than the classic Larkin length. This leads to the question: how individual defects contribute to the wall pinning. It is no wonder, therefore, that a simple "elastic" model which leads to the formulation of the Larkin length cannot – in most realistic cases – correctly describe the pinning behavior in martensitic, ferroelastic, and other ferroic domain structures (Fig. 1.14).

1.5 Conclusions

Multiferroic materials are well established. For some systems, such as $BiFeO_3$, industrial applications seem to be within our reach during the next decade. The key is a firm understanding of the coupling between the various order parameters in the bulk. The theory for the various mechanisms is also well established even in cases where the exact atomic nature of the coupling mechanism remains unclear. The open question is what new developments we can expect in the next 5 years?

The first development is to consider conductivity and even superconductivity as an equally important feature as multiferroicity. The treatment of high carrier densities and pairing mechanisms can follow the same path as the treatment of coupling between elastic, magnetic, and electric degrees of freedom.

Disruptive technologies can be envisaged if we succeed to use interfaces as active elements in multiferroic and other functional materials. This idea is new and finds its expression in the terminology of "domain boundary engineering." Theoretically, coupling between various properties in domain boundaries is easier than in the bulk: the coupling need not be related to terms such as $Q_1^2 Q_2^2$ in the relevant Hamiltonian (where Q is understood as an order parameter, which is constant over a length scale of several interatomic distances, at least). Instead, we have many more coupling phenomena at our disposal, such as the all important gradient coupling. Strong coupling such as seen in flexo-elasticity of the type $Q_1 \nabla Q_2$ and the interference of the gradient term $(\nabla Q)^2$ for each order parameter opens the door for a multitude of novel effects that contain hereto unknown structural states on a length scale of the thickness of interfaces (i.e. some nm). The same terms apply when we consider conducting interfaces that can play the role of electric wiring in devices.

References

1. E. Ascher, H. Rieder, H. Schmid, H. Stossel, Some properties of ferromagnetoelectric nickel-iodine boracite Ni3B7O13. J. Appl. Phys. **37**, 140 (1966)
2. S. Kinge, M. Crego-Calama, D.N. Reinhoudt, Self-assembling nanoparticles at surfaces and interfaces. ChemPhysChem **1**, 20 (2008)
3. M. Fiebig, Revival of the magnetoelectric effect. J. Appl. Phys. D **38**, R123 (2005)
4. J. Wang, J.B. Neaton, H. Zheng, V. Nagarajan, S.B. Ogale, B. Liu, D. Viehland, V. Vaithyanathan, D.G. Schlom, U.V. Waghmare, N.A. Spaldin, K.M. Rabe, M. Wuttig, R. Ramesh, Epitaxial BiFeO3 multiferroic thin film heterostructures. Science **299**, 1719 (2003)
5. A. Lubk, S. Gemming, N.A. Spaldin, First-principles study of ferroelectric domain walls in multiferroic bismuth ferrite. Phys. Rev. B **80**, art. 104110, (2009)
6. N.A. Spaldin, M. Fiebig, The renaissance of magnetoelectric multiferroics. Science **309**, 391 (2005)
7. J.B. Neaton, C. Ederer, U.V. Waghmare, N.A. Spaldin, K.M. Rabe, Elastic behavior associated with phase transitions in incommensurate Ba2NaNb5O15. Phys. Rev. B **71**, art. 014113 (2005)
8. E.K.H. Salje, Phase Transitions in ferroelastic and co-elastic crystals (Cambridge University Press, Cambridge, UK, 1993)
9. J.C. Lashley, S.M. Shapiro, B.L. Winn, et al., Observation of a continuous phase transition in a shape-memory alloy. Phys. Rev. Lett. **101**, art. 135703 (2008)
10. W. Eerenstein, N.D. Mathur, J.F. Scott, Multiferroic and magnetoelectric materials. Nature **442**, 759 (2006)
11. E.K.H. Salje, Multiferroic domain boundaries as active memory devices: Trajectories towards domain boundary engineering. ChemPhysChem **11**, 940 (2010)
12. S. Marais, V. Heine. C. Nex, et al., Phenomena due to strain coupling in phase – transitions. Phys. Rev. Lett. **66**, 2480 (1991)
13. M.A. Carpenter, E.K.H. Salje, Elastic anomalies in minerals due to structural phase transitions. Eur. J. Mineral. **10**, 693 (1998)
14. S.H. Lim, M. Murakami, W.L. Sarney, et al., The effects of multiphase formation on strain relaxation and magnetization in multiferroic BiFeO3 thin films. Adv. Func. Mater. **17**, 2594 (2007)
15. R.D. James, M. Wuttig, Magnetostriction of martensite. Phil Mag. A **77**, 1273 (1998)
16. K. Mori, M. Wuttig, Magnetoelectric coupling in terfenol-D/polyvinylidenedifluoride composites, Appl. Phys. Lett. **81**, 100 (2002)
17. J. Wang, J.B. Neaton, H. Zheng, et al., Epitaxial BiFeO3 multiferroic thin film heterostructures. Science **299**, 1719 (2002)
18. J. Seidel, L.W. Martin, Q. He, et al., Conduction at domain walls in oxide multiferroics. Nat. Mater. **8**, 229 (2009)
19. N. Hur, S. Park, P.A. Sharma, et al., Electric polarization reversal and memory in a multiferroic material induced by magnetic fields. Nature 429, 392 (2004)
20. C. Ederer, N.A. Spaldin, Weak ferromagnetism and magnetoelectric coupling in bismuth ferrite, Phys. Rev. B **71**, art. 060401 (2005)
21. A. Aird, E.K.H. Salje, Sheet superconductivity in twin walls: experimental evidence of WO3-x. J. Phys.: Condens. Matter **10**, L377 (1998)
22. B. Nagaraj, T. Sawhney, S. Perusse, et al., (BaSr)TiO3 thin films with conducting perovskite electrodes for dynamic random access memory applications. Appl. Phys. Lett. **74**, 3194 (1999)
23. S. Ramesh, V.P. Kumar, P. Kistaiah, et al., Preparation, characterization and thermo electrical properties of co-doped Ce0.8- xSM0.2CaxO2 (-) (delta) materials. Solid State Ionics **181**, 86 (2010)
24. T. Shimada, S. Tomoda, T. Kitamura, Ab initio study of ferroelectric closure domains in ultrathin PbTiO3 films. Phys. Rev. B **81**, art 144116 (2010)
25. S.E. Barnes, S. Maekawa, Current-spin coupling for ferromagnetic domain walls in fine wires. Phys. Rev. Lett. **95**, art. 107204 (2005)